Soft Matter

PAPER

View Article Online
View Journal | View Issue

Cite this: *Soft Matter*, 2014, **10**, 2600

Nanosecond lipid dynamics in membranes containing cholesterol

Clare L. Armstrong,[a] Wolfgang Häußler,[b] Tilo Seydel,[c] John Katsaras[def] and Maikel C. Rheinstädter*[ae]

Received 26th June 2013
Accepted 10th January 2014

DOI: 10.1039/c3sm51757h

www.rsc.org/softmatter

Lipid dynamics in the cholesterol-rich (40 mol%) liquid-ordered (l_o) phase of dimyristoylphosphatidylcholine membranes were studied using neutron spin-echo and neutron backscattering. Recent theoretical and experimental evidence supports the notion of the liquid-ordered phase in phospholipid membranes as a locally structured liquid, with small ordered 'domains' of a highly dynamic nature in equilibrium with a disordered matrix [S. Meinhardt, R. L. C. Vink and F. Schmid, *Proc. Natl. Acad. Sci. U. S. A.*, 2013, **110**(12), 4476–4481, C. L. Armstrong *et al.*, *PLoS One*, 2013, **8**(6), e66162]. This local structure was found to have a pronounced impact on the membranes' dynamical properties. We found that the long-wavelength dynamics in the liquid-ordered phase, associated with the elastic properties of the membranes, were faster by two orders of magnitude as compared to the liquid disordered phase. At the same time, collective nanoscale diffusion was significantly slower. The presence of a soft-mode (a slowing down) in the long-wavelength dispersion relationship suggests an upper size limit for the ordered lipid domain of ≈220 Å. Moreover, from the relaxation rate of the collective lipid diffusion of lipid–lipid distances, the lifetime of these domains was estimated to be about 100 nanoseconds.

1. Introduction

Cholesterol (Fig. 1a) is an essential component of eukaryotic cell membranes and is capable of modulating the membrane's permeability.[1] In association with rafts, cholesterol has been implicated in a variety of cell signalling processes.[2–6] Phase separation of cholesterol and other biomolecules (*e.g.*, sphingolipids, phospholipids, proteins) into functional domains is a key element of rafts.

Although much is known about lipid–cholesterol mixtures, this remains an active area of research due to cholesterol's role in domain formation.[7–15] It has been speculated that the 'stiff' cholesterol molecules align parallel to the hydrocarbon lipid tails, suppressing lipid tail fluctuations,[16] and in turn affecting the membrane's dynamical properties. Most lipid/cholesterol studies (see for example, ref. 7–12, 14 and 17) concur that, depending on the temperature and cholesterol concentration, four phases are observed, namely: (1) the gel phase ($L_{\beta'}$) at low temperatures; (2) the solid-ordered, $P_{\beta'}$ (ripple), phase;[18] (3) the liquid-disordered, L_α, phase; and (4) the liquid-ordered, l_o, phase. The solid-ordered (gel) and liquid-disordered (fluid) phases are well known from single component phospholipid bilayers; however, the liquid-ordered phase is only observed at high concentrations of cholesterol. This phase is somewhat peculiar as it appears to be well ordered (similar to the gel phase), but at the same time, its lipids diffuse at a rate similar to those found in fluid bilayers. The ripple ($P_{\beta'}$) phase was reported to disappear at high cholesterol contents.[19]

At low cholesterol contents, bilayers undergo a phase transition from the solid-ordered to the liquid-disordered phase, as

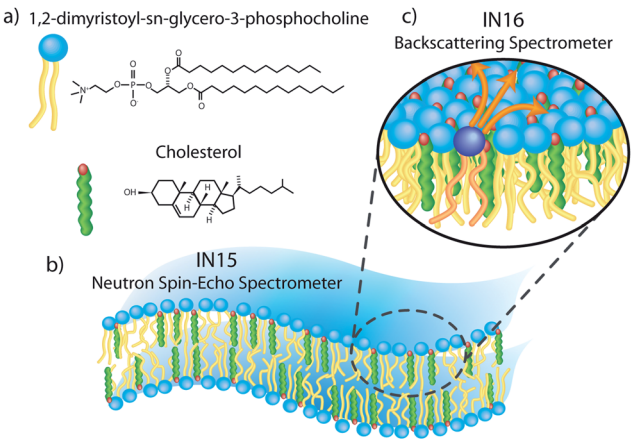

Fig. 1 (a) Schematic representation and molecular structures of DMPC and cholesterol molecules. (b) Picture of a DMPC–cholesterol lipid bilayer and its corresponding dynamical processes, as determined by neutron spin-echo and (c) neutron backscattering.

[a]*Department of Physics and Astronomy, McMaster University, Hamilton, ON, Canada. E-mail: rheinstadter@mcmaster.ca*
[b]*FRM-II & E21, Technische Universität München, Garching, Germany*
[c]*Institut Laue-Langevin, Grenoble, France*
[d]*Neutron Sciences Directorate, Oak Ridge National Laboratory, Oak Ridge, TN, USA*
[e]*Canadian Neutron Beam Centre, Chalk River, ON, Canada*
[f]*Joint Institute for Neutron Sciences, Oak Ridge, TN, USA*

is observed in pure lipid bilayers, and the temperature of the main transition, T_m, is slightly shifted towards higher temperatures. However, at high cholesterol concentrations ($\gtrsim$30 mol %), the main transition of l_o membranes is suppressed, while at intermediate cholesterol concentrations (*i.e.*, between about 10–30 mol%), most studies report a coexistence of $P_{\beta'}$ and l_o, or L_α and l_o phases.

Recently, Meinhardt, Vink and Schmid[13] reported a computer simulation study of a dipalmitoylphosphatidylcholine (DPPC)–cholesterol system. Using a coarse grained model that included 20 000 lipid molecules, a microemulsion-type state was observed containing nanometer-sized liquid-ordered domains in a liquid disordered environment. The existence of nanometer sized domains was also recently reported experimentally. Neutron diffraction experiments by Armstrong *et al.*[14] reported gel-like domains in equilibrium with a disordered matrix, which were thought to be saturated with cholesterol (66 mol%, in agreement with the umbrella model). The above-mentioned studies brought to light two important results. Firstly, that raft formation can occur in a binary system – it was previously thought that cholesterol in the presence of several different types of lipids was needed to form raft-like domains. Secondly, small, nanometer sized domains on the order of 100 Å were observed, in equilibrium with a disordered matrix.

In this paper we used dynamical neutron scattering techniques to study the dynamics of dimyristoylphosphatidylcholine (DMPC–40 mol% cholesterol) membranes in the liquid-ordered phase. By combining neutron spin-echo (NSE) and neutron backscattering (BS) data, long-wavelength elastic fluctuations, as well as dynamics on short lipid–lipid distances, were determined, giving insight into the dynamical processes of domain structures. From these results, an estimate of the size and lifetime of the lipid–cholesterol domains in phospholipid membranes was made.

2. Results

To determine lateral membrane dynamics, quasi-elastic in-plane neutron scattering was used to study the liquid-ordered phase of DMPC bilayers. The experiments were carried out at $T = 30$ °C and a D_2O relative humidity of 100%, ensuring full hydration of the membranes. Highly oriented, multilamellar DMPC membranes on a solid support containing 40 mol% cholesterol were used. Experiments were predominantly sensitive to the molecular dynamics of the lipid acyl chains, and their contribution to the scattering signal was enhanced by using the chain perdeuterated lipid DMPC-d54. The sample was aligned in the neutron beam such that one component of the momentum transfer was in the plane of the membranes. This in-plane component of the scattering vector is referred to as $\boldsymbol{q}_\parallel$.

2.1. Long-wavelength dynamics studied by neutron spin-echo spectrometry

Thermal fluctuations in lipid membranes, primarily using multilamellar stacks, have been investigated by thermal diffuse scattering, *i.e.*, X-ray lineshape analysis.[20,21] Elastic scattering led to a detailed understanding of the static properties of thermal fluctuations taking place in lipid membranes, including the membrane's elasticity which influences these fluctuations. According to linear smectic elasticity theory,[22,23] thermal fluctuations in the fluid phase of the membrane are governed by the free energy functional (Hamiltonian)

$$H = \int_A \mathrm{d}^2 r \sum_{n=1}^{N-1} \left(\frac{1}{2} \frac{B}{d_z} (u_{n+1} - u_n)^2 + \frac{1}{2} K d_z \left(\nabla_\parallel^2 u_n \right)^2 \right), \qquad (1)$$

where A denotes the area in the xy-plane, N is the number of bilayers, u_n is the deviation from the average position of the n-th bilayer, and d_z is the lamellar repeat spacing. B and $K = \kappa/d_z$ (κ denotes the bilayer bending rigidity) are elastic coefficients which govern the compression and bending modes of the smectic phase, respectively. A fundamental length scale in these systems is given by the smectic penetration length $\Lambda = \sqrt{K/B}$. Aligned lipid bilayers allow an independent determination of K and B.[24–26]

The mesoscopic scale fluctuations that are used to determine B and K occur in the nanosecond time range. As such, these moduli can be directly determined by measuring their corresponding fluctuation frequencies as a function of the scattering vector $\boldsymbol{q}_\parallel$. This can be achieved using the NSE technique, which is capable of probing nanometer length scales and nanosecond dynamics. NSE offers extremely high energy resolution through the Larmor 'tagging' of neutrons, and is in essence a measurement of neutron polarization[27] – as detailed in the Experimental section.

The fluctuation spectrum of a solid supported membrane stack was analytically modelled by Romanov and Ul'yanov.[28] Quasi-acoustic (quasi because the modes are not propagating due to the solid support) and optical modes were found with increasing fluctuation amplitudes towards the middle of the membrane stack. The layer fluctuations of lowest energy are the undulation modes, *i.e.*, highly correlated (conformal) layer displacements, which keep the inter-layer distances approximately constant.

Following the work of Ribotta[29] the dispersion is then calculated by

$$\tau^{-1}(\boldsymbol{q}_\parallel) = \frac{\kappa/d_z}{\eta_M} \boldsymbol{q}_\parallel^2 \frac{\boldsymbol{q}_\parallel^4 + (\pi/(\Lambda D))^2}{\boldsymbol{q}_\parallel^4 + \frac{1}{\mu\eta_M}(\pi/D)^2}, \qquad (2)$$

with η_M being an effective sliding viscosity and μ being a transport coefficient, $\mu = d_z^2/(12\eta_0)$ (η_0 is the viscosity of the solvent (water)).[29,30] This equation does not describe a pure undulation mode, which would be probed at q_z values of $q_z = 2\pi/d_z$, where d_z is the lamellar spacing, *i.e.* the distance between neighbouring membranes in the stack. If the scattering is probed at finite components $\Delta q_z = (q_z - 2\pi/d_z)$ or measured with coarse q_z resolution, there is mixing with baroclinic modes, which are distinctly slower than pure bilayer undulations as they involve a relocation motion of the water layer. The parameter D describes an effective finite size cut off length, which is related to the instrumental resolution $D = \pi/\Delta q_z$.

As shown by Bary-Soroker and Diamant,[31,32] additional slow dispersion branches with relaxation rates of hundreds of nanoseconds can be attributed to a surface relaxation mode, a

feature which is inherent in stacked membranes on a substrate. The corresponding dispersion relationship $\tau^{-1}(\boldsymbol{q}_\parallel)$ is set by the boundary conditions for the stress tensor at the stack surface:

$$\tau^{-1}(\boldsymbol{q}_\parallel) = \frac{2\gamma}{\theta\eta_M d_z}\left[\sinh^{-1}\left(\frac{1}{2}\theta^{1/2}|\boldsymbol{q}_\parallel|d_z\right) + \sinh^{-1}\left(\frac{1}{2}\theta^{-1/2}|\boldsymbol{q}_\parallel|d_z\right)\right], \quad (3)$$

where γ is the surface tension. As pointed out by Bary-Soroker and Diamant, γ in eqn (3) is a dynamic surface tension, in contrast to the static surface tension, $\gamma_{static} = \sqrt{KB}$. The general surface dynamics of membrane stacks depend on several restoring and dissipation mechanisms. Three moduli are associated with the restoring forces: the compression modulus B and bending modulus κ, which are also relevant for the bulk dynamics in eqn (2), as well as the surface tension γ. Viscous dissipation is characterized by three viscosity coefficients: η_M, η_T and η_V. η_M is the sliding viscosity, which is predominantly the viscosity of the water layer between two membranes in the membrane stack. η_T and η_V correspond to viscous response of the membranes. $\eta_{2D} = (\eta_T + \eta_V)d_z/2$ is an effective two-dimensional viscosity. θ is defined as $\theta = 2(\eta_T + \eta_V)/\eta_M$.

These two modes were previously observed in an NSE experiment using DMPC membranes,[30] *i.e.*, a fast, baroclinic mode of the bulk lamellar phase with relaxation rates of 0.01–0.1 μs^{-1} and a second, slower surface mode with relaxation rates of 1–10 μs^{-1}. The following results were obtained for DMPC at 30 °C: $\kappa = 14.8\ k_B T$ and $\eta_M = 0.016$ Pa s. B was calculated to be 2.0×10^{15} J m^{-4} (with $d_z = 54$ Å).

Additionally, a localized deviation from the undulation branch was observed at $T = 22$ °C, just above the main phase transition of deuterated DMPC, indicating a bilayer softening at a well defined wavenumber of $q_0 \approx 0.015$ Å^{-1}. The phospholipid membrane was 'softened' upon approaching T_m from the fluid phase, *i.e.* in the regime of critical swelling or anomalous swelling[33–35] at a length scale of $2\pi/q_\parallel \approx 420$ Å. Rheinstädter *et al.*[30] tentatively related this softening to the formation of solid-ordered (gel) and liquid-disordered (fluid) domains in the coexistence region, with bending occurring at the interface between two domains, as the corresponding elastic modulus is significantly reduced relative to the bending of a pure gel or fluid phase. Experimental evidence for the coexistence of gel and fluid nanodomains near the main phase transition has been recently reported[36] from neutron diffraction using the small coherence length of a neutron beam. In the past, it was thought that a single component membrane system exhibited pseudo-critical behaviour at the main phase transition (underwent a continuous second order phase transition) – the coexistence of gel and fluid domains is indicative of a classical first order phase transition.

Fig. 2 shows the intermediate scattering function (ISF) $I(\boldsymbol{q}_\parallel, t)/I(\boldsymbol{q}_\parallel, 0)$ for DMPC–40 mol% cholesterol. $\boldsymbol{q}_\parallel$ values in the interval 0.002 Å$^{-1} < \boldsymbol{q}_\parallel < 0.1$ Å^{-1} were measured, corresponding to length scales of 60 Å $< d <$ 3100 Å. Data were fitted using a single exponential decay,

$$I(\boldsymbol{q}_\parallel, t)/I(\boldsymbol{q}_\parallel, 0) = Ae^{-t/\tau}, \quad (4)$$

consistent with a single relaxation process. The resulting dispersion relationship is shown in Fig. 3. This relaxation is clearly dispersive. A soft mode appears in the dispersion, indicating a significant softening of the bilayer at a well defined wavenumber of $q_0 \approx 0.029$ Å^{-1} (corresponding to a length scale of $2\pi/0.029$ Å ≈ 220 Å), as shown by the dotted line in Fig. 3.

The solid line is a fit using eqn (3). A lamellar spacing of $d_z = 57.39$ Å was determined from reflectivity scans. η_M was fitted to $\eta_M = 0.0015$ Pa s, γ to $\gamma = 269.7$ mN m^{-1} and θ to $\theta = 422.2$. Bary-Soroker and Diamant presented a fit to the neutron experimental surface mode data by Rheinstädter *et al.* from pure DMPC bilayers, and determined values for θ, γ and η_M for the fluid and gel phases, as listed in Table 1.

In pure DMPC bilayers[30,32] a viscous water layer with a viscosity of $\eta_M = 0.016$ Pa s was reported, about 20 times the viscosity of bulk water. η_M in the presence of cholesterol of $\eta_M = 0.0015$ Pa s was only ≈2 times larger than the viscosity of bulk water at 25 °C of $\eta = 8.90 \times 10^{-4}$ Pa s. The membrane viscosities, $\eta_{T,V}$, determined by Bary-Soroker and Diamant[30,32] for pure DMPC were found to be 1.76 Pa s for the fluid phase, and 5.6 Pa s for the gel phase. The value for DMPC–40 mol% cholesterol was found to be significantly smaller, namely $\eta_{T,V} = 0.16$ Pa s.

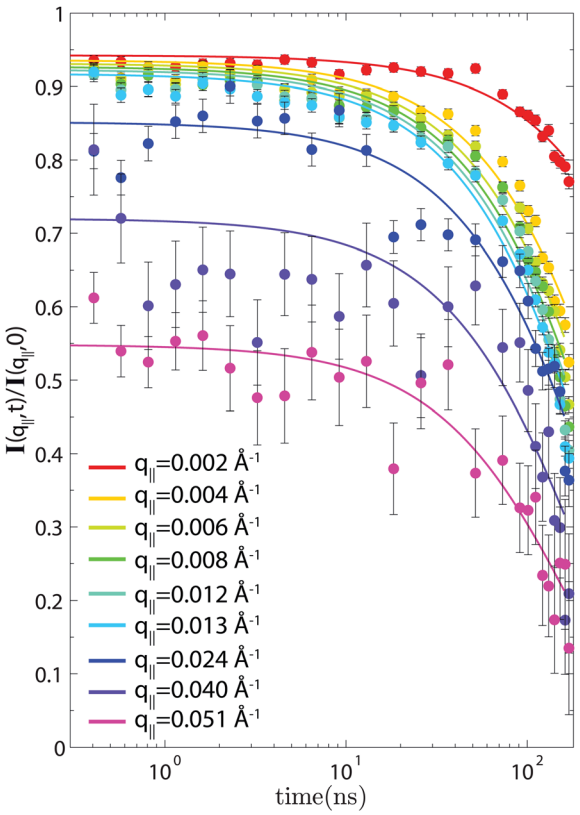

Fig. 2 The intermediate scattering function $I(\boldsymbol{q}_\parallel, t)/I(\boldsymbol{q}_\parallel, 0)$ was measured for $\boldsymbol{q}_\parallel$-values in the interval 0.002 Å$^{-1} < \boldsymbol{q}_\parallel <$0.1 Å^{-1}, corresponding to length scales of 60 Å $< d <$ 3100 Å. q_z was centred on the first Bragg reflection at $q_z = 0.109$ Å^{-1} for DMPC–40 mol% cholesterol bilayers. Selected $\boldsymbol{q}_\parallel$-values are shown as examples and show one pronounced relaxation process at about 100 ns. Solid lines in the figure represent least-square fits to the data using a single exponential decay. NSE data were collected at $T = 30$ °C.

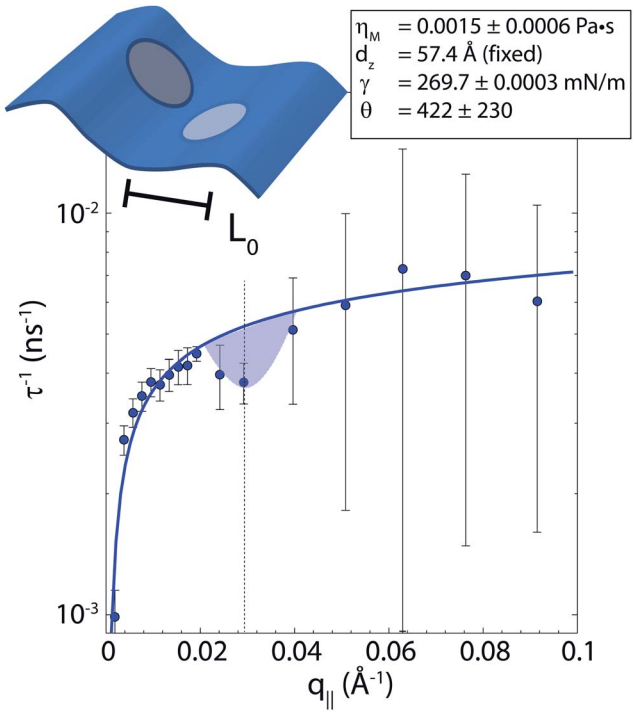

Fig. 3 Measured and theoretical dispersion relationships. Data are represented by symbols. A fit to eqn (3) is shown as a solid line. Fitted values for η_M, γ and θ are given in the figure with their corresponding errors. A soft mode was observed at a wavenumber of $q_0 \approx 0.029$ Å^{-1} ($\approx$220 Å), indicated by the dotted vertical line. The experimental dispersion relationship was determined from the data in Fig. 2 for DMPC–40 mol% cholesterol using the NSE technique at $T = 30$ °C.

The fitted values for θ and the surface tension γ in the l_o phase were significantly larger than the values determined for DMPC in its fluid ($\theta = 110$ and $\gamma = 5.4$ mN m^{-1}) phase. However, a θ of $\approx$420 is comparable to DMPC gel phase values of $\theta = 350$. Remarkably, the presence of cholesterol was found to increase the dynamic surface tension of the gel membrane stack by a factor of $\approx$10, from $\gamma = 28$ mN m^{-1} to $\gamma =$ 270 mN m^{-1}. As can be seen from eqn (3), this increase in γ leads to an increase of the relaxation rates of the surface mode, as compared to pure DMPC, suggesting much faster mesoscopic relaxation dynamics in membranes containing cholesterol.

2.2. Short-wavelength dynamics studied by the neutron backscattering technique

Neutron BS typically measures nanosecond dynamics from $\approx$3–15 Å, significantly smaller than those measured by NSE, enabling the determination of different types of motion.

The different dynamics can be distinguished based on their length scale dependence.[37–41] The nearest neighbour distance of hydration water molecules leads to a (coherent) correlation peak centered at 1.85 Å^{-1}, corresponding to a nearest neighbour distance of 3.4 Å between hydration water molecules. The lipid acyl chain correlation peak in DMPC is the result of the close packing of lipid tails in the hydrophobic membrane core. This correlation peak occurs at $\approx$1.5 Å^{-1} in the gel phase and at $\approx$1.4 Å^{-1} in fluid membranes,[36,38,42–50] corresponding to nearest neighbour distances of 4.8 Å and 5.2 Å, respectively (the tails form a hexagonally packed structure with $d_T = 4\pi/(\sqrt{3}q_T)$ (ref. 14)). Fast, picosecond dynamics on these length scales correspond to propagating, phonon-like dynamics,[46–51] while the slow, nanosecond dynamics relate to the motional coherence of the lipids.[52,53] These slow lipid dynamics were found to be coupled over $\approx$30 Å size patches, for times of up to tens of nanoseconds.[39,54,55] This coherent diffusion is relevant for the diffluence of domain structures and, therefore, for the lifetime of those domains. The corresponding scattering measured at the position of the lipid acyl tail correlation peak measures the diffluence of the tail pattern, while scattering measured at the lipid head group distance is sensitive to collective diffusion of the lipid molecules.

The quasi-elastic dynamics at $\boldsymbol{q}_{||}$ values corresponding to the positions of the lipid head group ($\boldsymbol{q}_{||} \approx 0.65$ Å^{-1}), the lipid acyl chain ($\boldsymbol{q}_{||} \approx 1.4$ Å^{-1}), and the hydration water ($\boldsymbol{q}_{||} \approx 1.9$ Å^{-1}) are shown in Fig. 4. The data were well fitted by two Lorentzians, *i.e.*, a two relaxation processes, τ_0 and τ_1, with an energy width (ΔE_{FWHM}) and the corresponding relaxation time $\tau = 2/(1.52 \times \Delta E_{FWHM})$, as derived in the Materials and Methods section. Because of the limited dynamical range of 15 μeV, the shortest time accessible was $\approx$0.1 ns, at which point the faster process, τ_1, was already partially out of the accessible time window, *i.e.*, the quasi-elastic broadening is slightly greater than the energy window. Because of this large uncertainty, we limit the discussion to τ_0, which falls perfectly into the backscattering time window. The resulting relaxation rates, ${\tau_0}^{-1}$, are depicted in Fig. 5. Data for pure DMPC are included for comparison.

While ${\tau_0}^{-1}$ for pure DMPC and DMPC–40 mol% cholesterol coincide at the water position at $\boldsymbol{q}_{||} = 1.9$ Å^{-1}, the ${\tau_0}^{-1}$ values increasingly differ for larger length scales (smaller $\boldsymbol{q}_{||}$ values). The relaxation rate at the lipid head group position was decreased by an order of magnitude, indicating that the collective diffusion for nearest neighbour distances of lipid molecules was retarded significantly in the presence of cholesterol. As the time for this relaxation process was previously reported to be $\approx$10 ns in pure DMPC,[39] potential domain structures in the liquid-ordered phase can be stable over $\approx$100 ns in the presence of cholesterol.

Table 1 Elastic parameters – as determined from fits of eqn (3) to the spin-echo data by Rheinstädter *et al.* in ref. 30 and 32, and from the data in Fig. 3

DMPC phase	d_z (Å)	η_M (Pa s)	$\eta_{T,V}$ (Pa s)	θ	γ (mN m^{-1})
Fluid[30,32]	54	0.016	1.76	110	5.4
Gel[30,32]	56	0.016	5.6	350	28
Liquid-ordered (40 mol%) [this work]	57.4 ± 0.02	0.0015 ± 0.0006	0.16 ± 0.15	422 ± 230	269.7 ± 0.0003

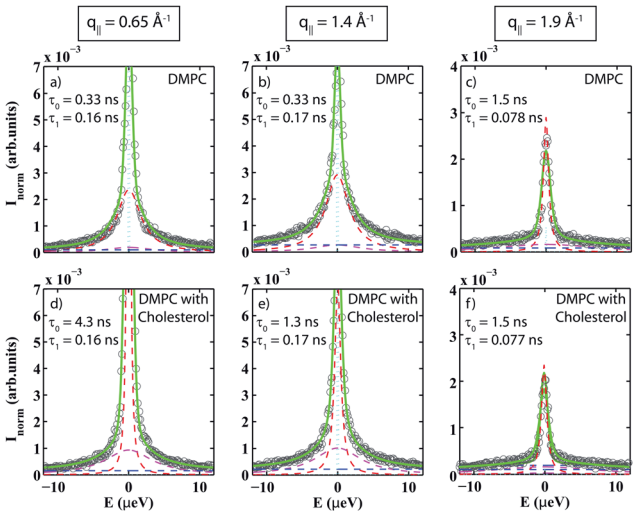

Fig. 4 Quasi-elastic scans at the lipid head group ($q_{||} \approx 0.65$ Å^{-1}), lipid acyl chain ($q_{||} \approx 1.4$ Å^{-1}) and water ($q_{||} \approx 1.9$ Å^{-1}) positions. Detectors were grouped to increase counting statistics. Detectors 1–3 were grouped to cover the $q_{||}$-range of the lipid–lipid correlation peak, *i.e.*, 0.48 Å^{-1} < $q_{||}$ <0.80 Å^{-1}. The inter acyl chain correlation peak was measured by detectors 9–13, which covered a $q_{||}$ range of 1.20 Å^{-1} < $q_{||}$ <1.60 Å^{-1}. The water contribution was detected using detectors 17–20 covering 1.78 Å^{-1} < $q_{||}$ <1.94 Å^{-1}. Two Lorentzians (red and magenta dashed lines) were used to describe the quasi-elastic broadening. A Dirac function (light blue dotted line) was used to describe the elastic intensity. This model was convoluted with the measured resolution function obtained from a vanadium standard. A flat background (blue dashed line) was subsequently added, and the result was used to fit the data (circles, fit result: green solid line). A flat background may arise from fast processes far beyond the accessible energy window of the spectrometer. The obtained relaxation times are given in the figures. The estimated error of the energy scale is ≈3%. $T = 30$ °C DMPC–40 mol% cholesterol data were collected using a BS spectrometer.

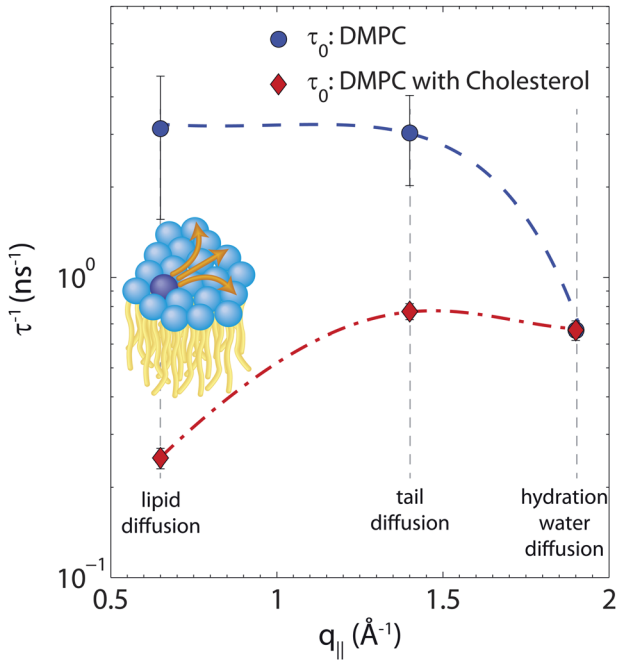

Fig. 5 Relaxation rates for DMPC/40 mol% cholesterol membranes at the lipid head group, lipid hydrocarbon chain and the water positions as determined from fits to the quasi-elastic data in Fig. 4. The error bars represent the fitting errors. Data were collected using a BS spectrometer at $T = 30$ °C. The dashed lines are guides to the eye.

3. Discussion

The lipid dynamics in the liquid-disordered phase of DMPC membranes containing 40 mol% cholesterol were studied using two different neutron scattering techniques. NSE gave access to long-wavelength dynamics and enabled the determination of the membrane's elastic properties. In a previous experiment using pure DMPC,[30] two dispersion branches were observed: a fast branch corresponding to the dynamics of baroclinic membrane modes and a second, slower branch corresponding to a surface mode. These modes are schematically shown in Fig. 6. The bilayers' bending and compressional modulus were determined by fitting theoretical dispersion curves to the experimental data. While it is well known that elastic parameters can be determined from elastic, diffuse X-ray and neutron scattering,[26] the origin of diffuse scattering is dynamic in nature. Quasi-elastic neutron scattering experiments can determine elastic parameters on different length scales, something which is crucial for developing molecular models of the underlying dynamics in order to compare with computer simulations.

The mesoscopic dynamics were found to be significantly faster in the presence of cholesterol and the relaxation rates of the baroclinic and surface modes increased by two orders of magnitude. Only the surface mode was observed in this study, as the baroclinic mode was too fast and not accessible by the IN15 spectrometer.

By fitting a theoretical dispersion relationship developed by Bary-Soroker and Diamant to the experimental data, the sliding viscosity η_M, the membrane viscosities $\eta_{T,V}$ and the dynamic viscosity γ were determined. The surface tension γ was found to have increased by a factor of 10, as compared to pure gel phase DMPC bilayers, leading to a drastic increase of relaxation rates. The values for θ in the presence of cholesterol were slightly larger than the θ values determined for DMPC in the gel phase. The membrane viscosities in Table 1 are in good agreement with the large range of values for η of 0.1 Pa s < η < 100 Pa s reported in the literature.[56–59] We note that because the values in Table 1 were determined using the same technique and model, these values can directly be compared. By fitting the data with eqn (3), we find that the viscosity of the l_o phase is lower than that in the gel or fluid phase DMPC bilayers. We also note that the viscosities in Table 1 were determined on length scales of 6–300 nm, a significantly smaller length scale than accessed by fluorescence experiments,[56–59] which are typically used for this type of experiments. The liquid-ordered phase was previously reported to combine the properties of gel and fluid phases, in other words, it is as well ordered as the gel phase, but 'softer' than the fluid phase, with a high diffusivity of lipid molecules. This also holds true on mesoscopic length scales.

The values for η_M in Table 1 are indicative of a reduction of the viscosity of the interstitial water layer in the presence of

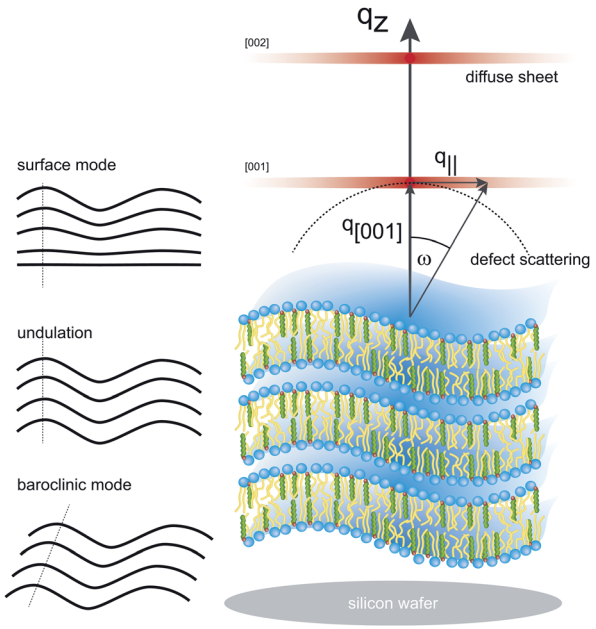

Fig. 6 Sketch of the NSE scattering geometry. Dynamics of the surface mode, the undulation mode and the baroclinic mode are observed as diffuse scattering sheets at q_z-positions of the reflectivity Bragg peaks ([001], [002], *etc.*). The spin-echo spectrometer was tuned to measure quasi-elastic scattering at several positions within the first diffuse sheet, as marked in the figure. The in-plane component of the total wave-vector transfer, $\boldsymbol{q}_{\|}$, was determined to be $\boldsymbol{q}_{\|} = q_{[001]} \tan(\omega)$. ω is the rocking angle, *i.e.*, the angle of sample rotation relative to the angle at which Bragg scattering occurred. The instrument was centred on the first order Bragg peak at $q_{[001]} = 0.109$ Å^{-1}.

cholesterol. The high value of the surface tension, γ, in the presence of cholesterol can directly be seen in the data, shown in Fig. 2 and 3, which has relaxation times about 10 times faster as compared to a pure lipid bilayer in ref. 30. This increase in γ is most likely related to the increase in order and restoring force due to cholesterol.

The viscosity of the interstitial water layer between the membranes strongly depends on the bilayer–water interaction. An increase in viscosity in the confined water, as compared to bulk water, was reported previously by Rheinstädter *et al.* in ref. 30, and is listed in Table 1. This observation is in agreement with a slowing down of the relaxation times of water molecules in the confined water layer, and a deviation from a pure Debye relaxation to a stretched exponential with an exponent of 0.75, indicative of a glassy system, as determined by Rheinstädter *et al.* in ref. 38. The presence of cholesterol is known to have two effects on lipid bilayers: the head group–head group distance and the d_z-spacing increase and the area per lipid decreases. This is well known as the condensation effect, and most likely leads to a smoother lipid–water interface, which may reduce the viscosity of the interstitial water layer.

Evidence for a heterogeneous structure of the liquid-ordered phase with ordered lipid nanodomains in equilibrium with a disordered membrane was recently provided both by theory and experiment. The computational work by Meinhardt, Vink and Schmid,[13] and the experimental studies by Armstrong *et al.*[14,50] were conducted using binary DPPC–cholesterol and DMPC–cholesterol systems – the identical system used for the spin-echo and backscattering experiments in this paper. The results can, therefore, be directly compared. Evidence for domains in DOPC–DPPC bilayers containing cholesterol has been recently presented by Sodt *et al.* from computer simulations and NMR.[61] As discussed recently by Rheinstädter and Mouritsen in ref. 15, the importance of observations of domains in these simple models is that domains were previously reported only from raft forming mixtures, which form stable equilibrium structures, not likely related to domains in real cells. The small and fluctuating domains observed in binary systems may be more closely related to what rafts are thought to be, as discussed for instance by Simons and Gerl in ref. 60. The spin-echo and backscattering data further characterize the dynamics of nanoscale, transient domains in binary phospholipid–cholesterol systems. Our spin-echo experiment was indirectly sensitive to the nano-domain structure: in pure DMPC, a soft-mode in the spin-echo dispersion was reported at a temperature close to the main transition. Coexisting gel and fluid domains were later reported in this critical regime, and the occurrence of the soft-mode could be linked to the existence of domains.

The observation of a softening in the liquid-ordered phase of DMPC (shown in Fig. 3) is consistent with the existence of ordered lipid domains, in a softer, disordered matrix. With the assumption that it is energetically more favourable to bend the membranes at the interface between domains, the length L_0 shown in Fig. 3 gives an upper limit for the domains of ≈ 220 Å.

The BS technique probed coherent dynamics on distances corresponding to the nearest neighbour lipid molecules. Such dynamics were previously related to a motional coherence in fluid lipid bilayers,[53] *i.e.*, the observation that slow nanosecond lipid dynamics are coupled over distances of 3–4 lipid diameters (≈ 30 Å) and over time scales of ≈ 10 ns. These dynamics can be thought of as the diffluence of the lipid backbone, related to a collective diffusion, and are very likely relevant to the formation and diffluence of domain structures.

The corresponding relaxation rates in Fig. 5 were found to significantly decrease (*i.e.*, by a factor of 13), as compared to pure DMPC bilayers. As the technique could not distinguish between lipid molecules in potentially highly ordered domains or in a disordered matrix, the obtained relaxation rates must be considered as mean rates, averaged over the two types of lipids. It can, therefore, be speculated that the diffluence of lipids participating in an ordered domain is slowed down even further, indicating domain patterns with life times on the order of hundreds of nanoseconds.

The coexistence of liquid-ordered and liquid-disordered domains in phospholipid membranes containing cholesterol was recently also reported from inelastic neutron scattering experiments.[50] In those experiments, the fast, picosecond nanoscale dynamics were probed and signals corresponding to liquid-disordered and liquid-ordered domains were observed simultaneously in DMPC membranes containing 40 mol% cholesterol. These phonon-like dynamics were observed as inelastic, propagating modes, in contrast to the overdamped, relaxation modes in Fig. 4. Instead of a uniform distribution of

cholesterol in the liquid-ordered phase, these results were indicative of a heterogeneous structure, with highly ordered cholesterol-rich domains in coexistence with fluid-like areas, in agreement with the findings presented here.

The effect of cholesterol on membrane elastic properties and diffusion was studied previously by diffuse X-ray scattering in DMPC, DPPC, SOPC, DOPC[42,45,62] and diC22:1, and dynamic neutron and light scattering in POPC bilayers.[63] NSE was used in the latter study and an increase in the bending elasticity with increasing cholesterol contents was observed. Pan *et al.*[42,62] found a dramatic increase in the membrane bending modulus as a function of cholesterol for saturated DMPC and DPPC bilayers from analysis of the diffuse scattering sheets at positions of the reflectivity Bragg peaks. The stiffening of the membranes led to faster dynamics on mesoscopic length scales in the presence of cholesterol, in excellent agreement with the results in the present study. We note that while bending elasticities can be determined with high precision from diffuse scattering experiments, complete dispersion relationships, such as in Fig. 3, can only be obtained from quasi-elastic experiments.

Our results can also be compared to results from recent molecular dynamics (MD) simulations in related phospholipid systems. MD simulations of a palmitoyloleoylphosphatidylcholine (POPC) membrane containing 40 mol% cholesterol[64] studied the time evolution of competing membrane structures (superlattice *versus* random) as a function of the molecular organization of cholesterol. The lateral distribution of cholesterol in the highly ordered ('superlattice') bilayer was found to be more stable than that of the random bilayer, suggesting an increased lifetime of cholesterol rafts, once they had formed.

The aggregation of cholesterol molecules in lipid bilayers and the formation of superlattice structures were also reported to depend on temperature, as well as the lipid concentration of the system.[65] In unsaturated POPC bilayers, the well depth of the free energy profile was calculated to be 3.5 kJ mol^{-1}, corresponding to the thermal energy (k_BT) at 310.15 K. This energy would, most likely, be drastically reduced in membranes made of saturated lipids, such as those in the present study.

The ordering effect of cholesterol on lipid acyl chains was also confirmed by MD simulations.[10,11,66] The presence of cholesterol was found to significantly reduce the *gauche*/*trans* ratio of hydrocarbon chains in neighbouring lipid molecules. Using this mechanism, cholesterol can induce structural changes in the bilayer through the formation of cholesterol-rich ordered lipid patches, in agreement with our experimental observations.

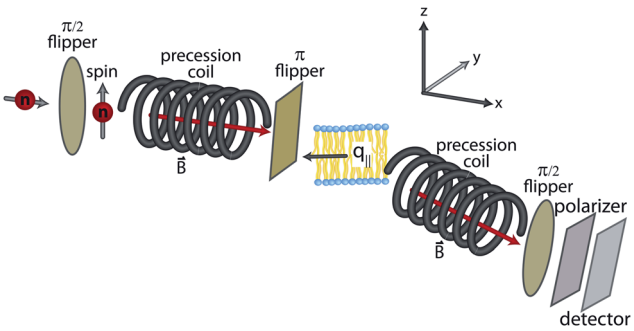

Fig. 8 Schematic of an NSE experiment. A π/2 flipper rotates the spin direction to be perpendicular to the scattering plane (*i.e.* along *z*). The neutron beam then travels through a magnetic field aligned along *x*. Before being scattered by the sample, the neutron spin is rotated by 180° around the *z* axis by the π flipper. The scattered neutrons travel through the second precession coil. A second π/2 flipper rotates the neutron spin into the *xy* plane. The final polarization of the beam is determined by using an analyzer–detector system.

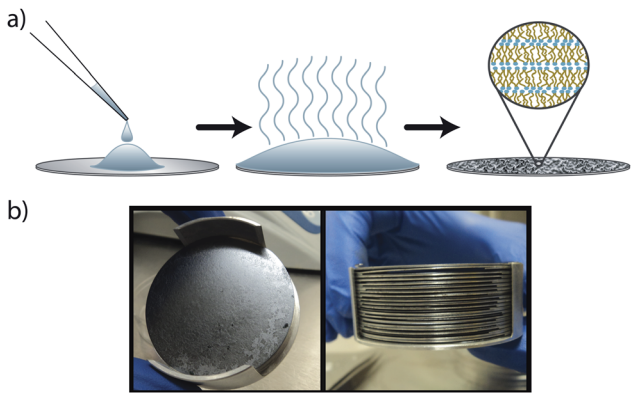

Fig. 7 Schematic of the sample preparation. (a) A DMPC–40 mol% cholesterol solvent solution was deposited onto Si wafers. The solvent was allowed to evaporate slowly, resulting in highly oriented bilayers. (b) The wafers were then sandwiched together with aluminium spacers, and hydrated with D_2O from the vapour phase.

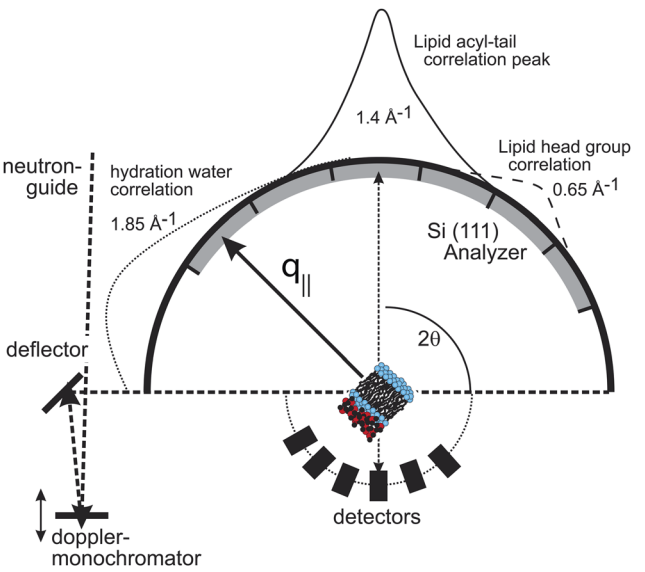

Fig. 9 Schematic of a BS setup.[37] An energy transfer of −15 μeV < *E* < +15 μeV could be scanned by varying the incident energy by Doppler-shifting the incident neutron energy through an adequate movement of the monochromator crystal. The nearest neighbour distance of the hydration water molecules leads to a correlation peak centered at 1.85 Å^{-1}. The lipid acyl chain correlation peak ≈1.4 Å^{-1} in fluid DMPC membranes is the result of the close packing of lipid tails in the hydrophobic membrane core. The average distance between two head groups leads to a correlation peak at $q_{||} \approx 0.65$ Å^{-1}.

4. Conclusion

In summary, the in-plane dynamics of liquid-ordered DMPC phospholipid membranes containing 40 mol% cholesterol were studied using quasi-elastic neutron scattering. Highly oriented, multilamellar membranes on a solid support were prepared and aligned in the neutron beam. Through selective deuteration, the system was tailored to be predominantly sensitive to the molecular dynamics of the lipid acyl chains. Moreover, by combining two different neutron scattering techniques, namely NSE and BS, the experiments covered length scales ranging from $\approx$3 to 3000 Angstroms.

NSE experiments were used to study membrane long-wavelength dynamics. The mesoscopic dynamics in the nanosecond time regime, as determined by the membrane's elastic parameters, were found to be faster by two orders of magnitude, as a result of a drastic increase in dynamic viscosity. However, membrane viscosity was significantly reduced with the addition of cholesterol. A soft-mode in the long-wavelength dispersion relationship corresponding to a length scale of $\approx$220 Å was tentatively related to the existence of ordered lipid domains in the liquid-ordered phase.

BS was used to study slow, nanosecond dynamics on nanometer length scales. The rate of collective diffusion on lipid–lipid distances was found to be significantly reduced in the presence of cholesterol. These dynamics were related to the diffluence of a domain pattern, and indicate that ordered domains can exist on time scales of several 100 nanoseconds.

Taken together with a previous inelastic neutron scattering study by Armstrong *et al.* (using a neutron triple-axis spectrometer),[50] the dynamical neutron scattering experiments of liquid ordered membranes cover length scales from Angstroms to almost a micrometre, and time scales from picoseconds to hundreds of nanoseconds. Different modes were observed, and the impact of cholesterol on membrane dynamics was quantified by measuring the corresponding dispersion relationships. A recent neutron diffraction study[14] together with computer-simulation calculations[13] provide strong evidence in favour of small-scale ordered lipid domains on the order of about 100 Å and with lifetimes up to about 100 nanoseconds. These domains, although in thermal equilibrium, are highly dynamic in nature and they are enriched in cholesterol in amounts of up to the theoretical saturation of 66% in agreement with the umbrella model.

5. Experimental

5.1. Sample preparation

Chain perdeuterated 1,2-dimyristoyl-*sn-glycero*-3-phosphocholine (DMPC-d54) and protonated cholesterol were used to enhance the inelastic scattering signal. Lipids and cholesterol were obtained from Avanti Polar Lipids Inc., AL, USA, and used without further purification. The lipid mixtures were hydrated using heavy water (D_2O, Sigma Aldrich, St. Louis, MO, USA). For short length scales, this type of sample preparation emphasizes the coherent scattering of the lipid acyl tails and hydration water, enabling the study of collective diffusion when using a neutron backscattering spectrometer. In the case of long length scales, the strong scattering contrast between the partially deuterated membrane core, protonated head group region, and deuterated hydration water layer enables one to study the long-wavelength dynamics of these interfaces through the membrane's elastic parameters.[30,37–39,52,53,67]

Highly oriented multi-lamellar stacks of 1,2-dimyristoyl-*sn-glycero*-3-phosphocholine (DMPC) with 40 mol% cholesterol were deposited onto 2″ (diameter 5.08 cm) single-side polished Si wafers with a thickness of 300 μm. A solution of 20 mg mL^{-1} DMPC with 40 mol% cholesterol in 1 : 1 chloroform and 2,2,2-trifluoroethanol (TFE) was prepared. The Si wafers were cleaned by alternate 12 minute sonications in ultra pure water and ethanol at 313 K. This process was repeated twice. As depicted in Fig. 7(a), 1 mL of the lipid solution was pipetted onto each Si wafer and allowed to dry. The wafers were kept under vacuum overnight to remove all traces of the solvent. The samples were then hydrated with heavy water, D_2O, and annealed in an incubator at 308 K for 24 hours. Following this protocol, each wafer contained roughly 3000 highly oriented stacked membranes with a total thickness of $\approx$10 μm. The sample had a total mass of about 400 mg of DMPC–cholesterol.

Twenty such Si wafers were stacked with 0.6 mm aluminium spacers placed in between each wafer to allow for the membranes to hydrate during the experiment (see Fig. 7(b)). For the spin-echo measurements, the 'sandwich' sample was kept in a sealed temperature and humidity controlled aluminum chamber. Hydration of lipid membranes from water vapour was achieved by independently adjusting the temperature of the heavy water reservoir, the sample and the chamber cover. Temperature and humidity sensors were installed close to the sample. A water bath was used to control the temperature of the different water reservoirs, and the temperatures of the sample and its cover were controlled using Peltier elements. For the backscattering experiments the sample was mounted in a hermetically sealed aluminium container residing in a cryostat, and hydrated from D_2O vapor. Saturation of the vapor in the voids around the lipids was assured by placing a piece of pulp soaked in D_2O within the sealed sample container. The pulp was shielded by cadmium to exclude any parasitic contribution to the scattering.

The sample was mounted vertically in the neutron beam such that a component of the momentum transfer could either be placed in the plane of the membrane ($\boldsymbol{q}_{\parallel}$), or perpendicular to it ($\boldsymbol{q}_z$). Out-of-plane and in-plane structure and dynamics could be measured by simply rotating the sample by 90°, as shown in Fig. 8 and 9.

The temperature of the main transition, T_m, in DMPC-d54 was reported to occur at $T \approx 294.7$ K ($\approx$21.5 °C) in fully hydrated multi-lamellar DMPC systems,[37,68] a value slightly lower than its protonated counterpart of $T_m = 296.6$ K (23.4 °C). All measurements reported here were carried out at $T = 303$ K (30 °C), well above T_m.

5.2. Neutron spin-echo experiment

Neutron spin-echo (NSE) spectrometry, developed by Ferenc Mezei,[27] is a technique that is commonly used for the study of

soft matter systems.[69] It is capable of monitoring the slowest time scales (as slow as hundreds of nanoseconds), by using neV energy resolution. The high resolution provided by NSE is the result of decoupling the energy resolution from the wavelength band width. A key feature which differentiates NSE from other neutron scattering techniques is that the characteristic quantity measured is the intermediate scattering function, $I(Q, t)$, rather than $S(Q, E)$, giving direct access to the relaxation time, τ. Fig. 8 shows a sketch of a typical NSE experimental setup.

Commonly, the incoming neutron beam with a wavelength spread of 15% (FWHM) is polarized along the neutron's velocity direction (x in Fig. 8). At the front end of the instrument, a $\pi/2$ flipper rotates the spin direction to be perpendicular to the scattering plane (*i.e.* along z). The neutron beam then travels within the first precession coil through a magnetic field aligned along x. Thus, the spins perform a Larmor precession with frequency ω_L in the yz plane. The angle between the neutron spin direction at the beginning and end of the first precession coil depends on the time spent within the magnetic field, and hence on its velocity. Before being scattered by the sample, the neutron spin is rotated by 180° around the z axis by the π flipper. The neutrons are then scattered by the sample and travel through the second precession coil within a magnetic field equal to that of the first coil. Inside the second coil, the Larmor precession effectively unwinds the neutron spin. If the scattering event is elastic, the unwinding of the neutron spin is perfect. A second $\pi/2$ flipper rotates the neutron spin into the xy plane. The final polarization of the beam is determined by the analyzer–detector system.

Therefore, a neutron spin-echo spectrometer essentially measures the change in neutron polarization. If all scattering is elastic (no velocity change occurs as a result of sample interaction), then the precession angle of a neutron through the first coil, ϕ_1, will be the same as the precession angle through the second coil, ϕ_2, as long as $B_1 = B_2$. Elastic scattering will result in a total precession angle of $\Delta\phi = \phi_1 - \phi_2 = 0$ for all incoming neutron velocities, and the initial polarization can be retrieved.

If inelastic scattering occurs, the scattered neutrons will have a different distribution of velocities and will precess through different angles in the second coil, thereby creating a distribution of spin angles about z-axis after precession ($\Delta\phi \neq 0$). The angular distribution of scattered neutrons leads to a decrease in the detected neutrons after spin analysis, as not all neutrons will return to their initial polarization. If the neutron experiences a small energy transfer ΔE, there will be a linear change in $\Delta\phi$ ($\Delta\phi = \tau \times \omega_L$), with τ being a real time.[70] By slightly varying the strength of B_1 and B_2, the polarization of the neutron beam can be measured for different Fourier times τ. When normalized to a perfectly elastic scatterer, such as for example graphite, the polarization is directly related to the intermediate scattering function, $I(Q, t)$. In the case of a quasi-elastic response with a Lorentzian lineshape of half-width Γ, the polarization will exhibit a single exponential decay,

$$P_{NSE} = \frac{I(Q,t)}{I(Q,0)} = e^{-t/\tau}. \quad (5)$$

Spin-echo experiments were carried out using the IN15 spectrometer situated at the cold source of the high flux reactor of the Institut Laue-Langevin (ILL) in Grenoble, France. The experiment used a wavelength band centered at $\lambda = 15$ Å, with a $\Delta\lambda/\lambda = 15\%$ set by a velocity selector. In order to normalize the ISF and to correct for the instrumental resolution, $I(Q, t)$ was divided by a measurement from graphite, a perfectly elastic scatterer on the length and time scales investigated here.

The sample was placed in a humidity chamber, which was capable of controlling the sample temperature to an accuracy of ±0.1 K. The sample was mounted vertically in the neutron beam such that a component of the scattering vector ($\vec{Q}$) could either be placed in the membrane plane ($\boldsymbol{q}_\parallel$), or perpendicular to the membrane ($\boldsymbol{q}_z$), by simply rotating the sample by 90°. In this way, out-of-plane and in-plane scans could be easily measured.

The lamellar repeat spacing of multi-lamellar membranes was determined by measuring reflectivity scans *in situ*. The NSE spectrometer was used in diffraction mode, with the $\pi/2$ flippers turned off, and the reported data are the average of the NSF and SF counts. A d_z-spacing of 57.39 ± 0.02 Å was determined, which corresponds to a hydration of 99.8% RH, close to full hydration of the bilayers.[35] The quality of the sample was further checked in rocking scans and the mosaicity of the membranes, *i.e.*, the orientation between membranes in the same stack and membranes on different silicon wafers in the sandwich was determined to be less than 1°.

Neutron spin-echo in oriented membranes is an established technique to study elastic properties and diffusion.[30,71,72] As in a previous neutron spin-echo experiment with oriented membranes by Rheinstädter *et al.*,[30] we have measured spin-echo curves on the first diffuse Bragg sheet as a function of $\boldsymbol{q}_\parallel$, *i.e.*, at constant $q_z = 2\pi/d_z$. A sketch of the scattering geometry is shown in Fig. 6a. The in plane component of the scattering vector was calculated to be $q_\parallel = q_{[001]} \tan(\omega)$, with $q_{[001]} = 0.109$ Å^{-1} for the first reflectivity Bragg peak. ω is the rocking angle, *i.e.*, the sample rotation with respect to the specular Bragg angle.

5.3. Neutron backscattering experiment

Neutron backscattering offers a method of measuring the inelastic scattering in a system over a broad dynamic range ($\approx 10^2$ μeV) with a very high energy resolution ($\approx$0.1–20 μeV).[73] This energy range corresponds to dynamics occurring in the nanosecond regime,[74] bridging the gap between the short picosecond time scales, measured by time-of-flight (TOF) spectrometers and the long 10–100 ns regime accessible using NSE. This particular range makes it a useful tool for the study of motions in lipid membrane systems. For many neutron spectrometers, the energy resolution is improved by creating a well-defined monochromatic incident beam; however, this often results in a low neutron flux. The characteristic feature of the backscattering geometry is that high energy resolution is achieved by using a Bragg angle (2θ) close to 180° (hence, 'backscattering') for the analysis of the scattered neutron wavelength, which is achieved with a bank of analyzer crystals. The backscattering condition yields an extremely well defined wavelength (or energy) resolution of the beam. This property can be seen directly by the differentiation of Bragg's law:

$$\lambda = 2d \sin\theta,$$

$$\frac{\Delta\lambda}{\lambda} = \frac{\Delta d}{d} + \frac{\Delta\theta}{\tan\theta}. \quad (6)$$

As θ goes to 90°, $\tan\theta$ approaches ∞, making the second term in eqn (6) negligible. The wavelength resolution is now, to first order, independent of the beam divergence, $\Delta\theta$, and is only dependent on the Darwin width of the monochromator and analyzer crystal, Δd. The resolution is optimized by using perfect, silicon crystals with $\Delta d/d$ values on the order of 10^{-4}.[74,75]

The experiments were carried out using the cold neutron backscattering spectrometer IN16 (ref. 75) at the Institut Laue-Langevin (ILL) with an energy resolution of about 0.9 μeV FWHM ($\lambda = 6.27$ Å). An energy transfer of -15 μeV $< E <$ +15 μeV could be scanned by varying the incident energy by Doppler-shifting the incident neutron energy through an adequate movement of the monochromator crystal. Twenty detectors in exact backscattering geometry with respect to the analyzer crystals, each covering an angular width of 6.5° were used. A Q range of 0.43 Å^{-1} < Q < 1.92 Å^{-1} was scanned, accessing time scales of about 0.1 ns < t < 1.5 ns and length scales of 3.2 Å < d < 14.6 Å. The samples were mounted in a hermetically sealed aluminum container within a helium cryostat with an accuracy of ±0.1 K and hydrated from D_2O. By aligning the bilayer normal at 135° with respect to the incoming neutron beam, the momentum transfer could be placed in the plane of the bilayers ($\boldsymbol{q}_\parallel$). The experimental setup is shown in Fig. 9.

5.4. Energy-τ conversion

The relaxation times obtained by NSE were converted to quasi-elastic broadening values using

$$\Delta E_{\mathrm{FWHM}} = \frac{2\hbar}{\tau}, \quad (7)$$

which can be obtained by Fourier transforming the intermediate scattering function, resulting in a Lorentzian function with a FWHM that is the quasi-elastic energy broadening. The scattering function $S(\boldsymbol{q}_\parallel, t)$ is defined by:

$$S(\boldsymbol{q}_\parallel, \omega) = \frac{1}{2\pi\hbar}\int I(\boldsymbol{q}_\parallel, t)\mathrm{e}^{-\mathrm{i}\omega t}\mathrm{d}t \quad (8)$$

For a single exponential decay, $I(\boldsymbol{q}_\parallel, t) = \mathrm{e}^{-t/\tau}$,

$$S(\boldsymbol{q}_\parallel, \omega) = \frac{1}{2\pi\hbar}\int_\infty^\infty \mathrm{e}^{-t/\tau}\mathrm{e}^{-\mathrm{i}\omega t}\mathrm{d}t = \frac{1}{2\pi\hbar}\int_\infty^\infty \mathrm{e}^{-t/\tau-\mathrm{i}\omega t}\mathrm{d}t, \quad (9)$$

which is integrated to

$$S(\boldsymbol{q}_\parallel, \omega) = \frac{1}{\pi}\left(\frac{\frac{\hbar}{\tau}}{\left(\frac{\hbar}{\tau}\right)^2 + (\hbar\omega)^2}\right). \quad (10)$$

This equation is a Lorentzian function with a HWHM of $\frac{\hbar}{\tau}$. Therefore, the FWHM energy broadening of the scattering function is given as:

$$\Delta E_{\mathrm{FWHM}} = \frac{2\hbar}{\tau}\frac{10^{15}}{e} = \frac{2}{1.52\tau}, \quad (11)$$

where the units of ΔE_{FWHM} and τ are μeV and ns, respectively.

Acknowledgements

This research was funded by the Natural Sciences and Engineering Research Council (NSERC) of Canada, the National Research Council (NRC), the Canada Foundation for Innovation (CFI), and the Ontario Ministry of Economic Development and Innovation. J.K. acknowledges support from the Scientific User Facilities Division of the Office of Basic Energy Sciences (BES), and the Laboratory Directed Research and Development (LDRD) program of Oak Ridge National Laboratory, managed by UT-Battelle, LLC, for the U.S. Department of Energy (DOE) under contract no. DE-AC05-00OR2275. M.C.R. is the recipient of an Early Researcher Award from the Province of Ontario.

References

1 G. Szabo, *Nature*, 1974, **252**, 47–49.
2 K. Simons and E. Ikonen, *Nature*, 1997, **387**, 569–572.
3 D. A. Brown and E. London, *J. Biol. Chem.*, 2000, **275**, 17221.
4 R. Petrie, P. Schnetkamp, K. Patel, M. Awasthi-Kalia and J. Deans, *J. Immunol.*, 2000, **165**, 1220.
5 B. Papanikolaou, A. Papafotika, C. Murphy, T. Papamarcaki, O. Tsolas, M. Drab, T. V. Kurzchalia, M. Kasper and S. Christoforidis, *J. Biol. Chem.*, 2005, **28**, 26406.
6 L. Pike, *J. Lipid Res.*, 2006, **47**, 1597.
7 R. Vist and J. H. Davis, *Biochemistry*, 1990, **29**, 451.
8 P. Almeida, W. Vaz and T. Thompson, *Biochemistry*, 1992, **31**, 6739–6747.
9 J. L. Thewalt and M. Bloom, *Biophys. J.*, 1992, **63**, 1176–1181.
10 F. de Meyer and B. Smit, *Proc. Natl. Acad. Sci. U. S. A.*, 2009, **106**, 3654–3658.
11 F. J.-M. de Meyer, A. Benjamini, J. M. Rodgers, Y. Misteli and B. Smit, *J. Phys. Chem. B*, 2010, **114**, 10451–10461.
12 D. Marsh, *Biochim. Biophys. Acta, Biomembr.*, 2010, **1798**, 688–699.
13 S. Meinhardt, R. L. C. Vink and F. Schmid, *Proc. Natl. Acad. Sci. U. S. A.*, 2013, **110**, 4476–4481.
14 C. L. Armstrong, D. Marquardt, H. Dies, N. Kučerka, Z. Yamani, T. A. Harroun, J. Katsaras, A.-C. Shi and M. C. Rheinstädter, *PLoS One*, 2013, **8**, e66162.
15 M. C. Rheinstädter and O. G. Mouritsen, *Curr. Opin. Colloid Interface Sci.*, 2013, **18**, 440–447.
16 T. Róg, M. Pasenkiewicz-Gierula, I. Vattulainen and M. Karttunen, *Biochim. Biophys. Acta*, 2009, **1788**, 97–121.
17 M. A. Barrett, S. Zheng, L. A. Toppozini, R. J. Alsop, H. Dies, A. Wang, N. Jago, M. Moore and M. C. Rheinstädter, *Soft Matter*, 2013, **9**, 9342–9351.
18 J. Katsaras, S. Tristram-Nagle, Y. Liu, R. Headrick, P. Fontes, E. Mason and J. Nagle, *Phys. Rev. E: Stat. Phys., Plasmas, Fluids, Relat.*, 2000, **61**, 5668–5677.
19 A. Hicks, M. Dinda and M. A. Singer, *Biochim. Biophys. Acta, Biomembr.*, 1987, **903**, 177–185.
20 C. R. Safinya, D. Roux, G. S. Smith, S. K. Sinha, P. Dimon, N. A. Clark and A. M. Bellocq, *Phys. Rev. Lett.*, 1986, **57**, 2718–2721.

21 H. I. Petrache, N. Gouliaev, S. Tristram-Nagle, R. Zhang, R. M. Suter and J. F. Nagle, *Phys. Rev. E: Stat. Phys., Plasmas, Fluids, Relat.*, 1998, **57**, 7014–7024.
22 A. Caillé, *C. R. Seances Acad. Sci., Ser. B*, 1972, **274**, 891–893.
23 N. Lei, C. Safinya and R. Bruinsma, *J. Phys. II*, 1995, **5**, 1155–1163.
24 Y. Lyatskaya, Y. Liu, S. Tristram-Nagle, J. Katsaras and J. F. Nagle, *Phys. Rev. E: Stat. Phys., Plasmas, Fluids, Relat.*, 2000, **63**, 011907.
25 T. Salditt, M. Vogel and W. Fenzl, *Phys. Rev. Lett.*, 2003, **90**, 178101.
26 G. Pabst, N. Kučerka, M.-P. Nieh, M. Rheinstädter and J. Katsaras, *Chem. Phys. Lipids*, 2010, **163**, 460–479.
27 *Neutron Spin Echo*, ed. F. Mezei, Springer, Berlin, 1980.
28 V. Romanov and S. Ul'yanov, *Phys. Rev. E: Stat. Phys., Plasmas, Fluids, Relat.*, 2002, **66**, 061701.
29 R. Ribotta, D. Salin and G. Durand, *Phys. Rev. Lett.*, 1974, **32**, 6–9.
30 M. C. Rheinstädter, W. Häussler and T. Salditt, *Phys. Rev. Lett.*, 2006, **97**, 048103.
31 H. Bary-Soroker and H. Diamant, *Europhys. Lett.*, 2006, **73**, 871–877.
32 H. Bary-Soroker and H. Diamant, *Phys. Rev. E: Stat. Phys., Plasmas, Fluids, Relat.*, 2007, **76**, 042401.
33 P. Mason, J. Nagle, R. Epand and J. Katsaras, *Phys. Rev. E: Stat. Phys., Plasmas, Fluids, Relat.*, 2001, **63**, 030902R.
34 G. Pabst, J. Katsaras, V. A. Raghunathan and M. Rappolt, *Langmuir*, 2003, **19**, 1716–1722.
35 N. Chu, N. Kučerka, Y. Liu, S. Tristram-Nagle and J. F. Nagle, *Phys. Rev. E: Stat. Phys., Plasmas, Fluids, Relat.*, 2005, **71**, 041904.
36 C. L. Armstrong, M. A. Barrett, L. Toppozini, N. Kučerka, Z. Yamani, J. Katsaras, G. Fragneto and M. C. Rheinstädter, *Soft Matter*, 2012, **8**, 4687–4694.
37 M. C. Rheinstädter, T. Seydel, F. Demmel and T. Salditt, *Phys. Rev. E: Stat. Phys., Plasmas, Fluids, Relat.*, 2005, **71**, 061908.
38 M. C. Rheinstädter, T. Seydel and T. Salditt, *Phys. Rev. E: Stat. Phys., Plasmas, Fluids, Relat.*, 2007, **75**, 011907.
39 M. C. Rheinstädter, J. Das, E. J. Flenner, B. Brüning, T. Seydel and I. Kosztin, *Phys. Rev. Lett.*, 2008, **101**, 248106.
40 L. Toppozini, C. L. Armstrong, M. D. Kaye, M. Tyagi, T. Jenkins and M. Rheinstädter, *ISRN Biophys.*, 2012, **2012**, 520307.
41 L. Toppozini, C. L. Armstrong, M. A. Barrett, S. Zheng, L. Luo, H. Nanda, V. Garcia Sakai and M. Rheinstädter, *Soft Matter*, 2012, **8**, 11839–11849.
42 J. Pan, T. T. Mills, S. Tristram-Nagle and J. F. Nagle, *Phys. Rev. Lett.*, 2008, **100**, 198103.
43 T. T. Mills, G. E. S. Toombes, S. Tristram-Nagle, D.-M. Smilgies, G. W. Feigenson and J. F. Nagle, *Biophys. J.*, 2008, **95**, 669–681.
44 T. Mills, S. Tristram-Nagle, F. Heberle, N. Morales, J. Zhao, J. Wu, G. Toombes, J. Nagle and G. Feigenson, *Biophys. J.*, 2008, **95**, 682–690.
45 T. Mills, J. Huang, G. Feigenson and J. Nagle, *Gen. Physiol. Biophys.*, 2009, **28**, 126–139.
46 M. C. Rheinstädter, C. Ollinger, G. Fragneto, F. Demmel and T. Salditt, *Phys. Rev. Lett.*, 2004, **93**, 108107.
47 M. C. Rheinstädter, C. Ollinger, G. Fragneto and T. Salditt, *Phys. B*, 2004, **350**, 136–139.
48 B. Brüning, M. C. Rheinstädter, A. Hiess, B. Weinhausen, T. Reusch, S. Aeffner and T. Salditt, *Eur. Phys. J. E*, 2010, **31**, 419–428.
49 M. D. Kaye, K. Schmalzl, V. C. Nibali, M. Tarek and M. C. Rheinstädter, *Phys. Rev. E: Stat. Phys., Plasmas, Fluids, Relat.*, 2011, **83**, 050907.
50 C. L. Armstrong, M. A. Barrett, A. Hiess, T. Salditt, J. Katsaras, A.-C. Shi and M. C. Rheinstädter, *Eur. Biophys. J.*, 2012, **41**, 901–913.
51 S. Chen, C. Liao, H. Huang, T. Weiss, M. Bellisent-Funel and F. Sette, *Phys. Rev. Lett.*, 2001, **86**, 740–743.
52 M. C. Rheinstädter, T. Seydel, W. Häußler and T. Salditt, *J. Vac. Sci. Technol., A*, 2006, **24**, 1191–1196.
53 M. C. Rheinstädter, *Biointerfaces*, 2008, **3**, FB83–FB90.
54 E. Falck, T. Róg, M. Karttunen and I. Vattulainen, *J. Am. Chem. Soc.*, 2008, **130**, 44–45.
55 S. Busch, C. Smuda, L. Pardo and T. Unruh, *J. Am. Chem. Soc.*, 2010, **132**, 3232–3233.
56 R. Peters and R. J. Cherry, *Proc. Natl. Acad. Sci. U. S. A.*, 1982, **79**, 4317–4321.
57 W. Vaz, J. Stümpel, D. Hallmann, A. Gambacorta and M. Rosa, *Eur. Biophys. J.*, 1987, **15**, 111–115.
58 Y. Gambin, R. Lopez-Esparza, M. Reffay, E. Sierecki, N. S. Gov, M. Genest, R. S. Hodges and W. Urbach, *PNAS*, 2006, **103**, 2098–2102.
59 P. Cicuta, S. L. Keller and S. L. Veatch, *J. Phys. Chem. B*, 2007, **111**, 3328–3331.
60 K. Simons and M. J. Gerl, *Nat. Rev. Mol. Cell Biol.*, 2010, **11**, 688–699.
61 A. J. Sodt, M. L. Sandar, K. Gawrisch, R. W. Pastor and E. Lyman, *J. Am. Chem. Soc.*, 2014, **136**, 725–732.
62 J. Pan, S. Tristram-Nagle and J. F. Nagle, *Phys. Rev. E: Stat. Phys., Plasmas, Fluids, Relat.*, 2009, **80**, 021931.
63 L. R. Arriaga, I. López-Montero, F. Monroy, G. Orts-Gil, B. Farago and T. Hellweg, *Biophys. J.*, 2009, **96**, 3629–3637.
64 Q. Zhu, K. H. Cheng and M. W. Vaughn, *J. Phys. Chem. B*, 2007, **111**, 11021–11031.
65 Y. Andoh, K. Oono, S. Okazaki and I. Hatta, *J. Chem. Phys.*, 2012, **136**, 155104.
66 S. A. Pandit, G. Khelashvili, E. Jakobsson, A. Grama and H. Scott, *Biophys. J.*, 2007, **92**, 440–447.
67 M. C. Rheinstädter, T. Seydel, B. Farago and T. Salditt, *J. Neutron Res.*, 2006, **14**, 257–268.
68 M. Weik, U. Lehnert and G. Zaccai, *Biophys. J.*, 2005, **89**, 3639–3646.
69 D. Richter, M. Monkenbusch, A. Arbe and J. Colmenero, *Neutron Spin Echo in Polymer Systems*, Springer, Berlin, Heidelberg, 2005, vol. 174, pp. 1–221.
70 M. C. Rheinstädter, in *Dynamics of Soft Matter*, ed. V. Garca Sakai, C. Alba-Simionesco and S.-H. Chen, Springer, US, 2012, pp. 263–286.
71 W. Pfeiffer, S. König, J. Legrand, T. Bayerl, D. Richter and E. Sackmann, *Europhys. Lett.*, 1993, **23**, 457–462.

72 C. L. Armstrong, L. Toppozini, H. Dies, A. Faraone, M. Nagao and M. C. Rheinstädter, *ISRN Biophys.*, 2013, **2013**, 439758.
73 T. Salditt and M. Rheinstädter, in *Structure and Dynamics of Model Membrane Systems Probed by Elastic and Inelastic Neutron Scattering*, ed. J. Fitter, T. Gutberlet and J. Katsaras, Springer, Heidelberg, 2006, pp. 503–530.
74 E. Mamontov and K. Herwig, *Rev. Sci. Instrum.*, 2011, **82**, 085109.
75 B. Frick and M. Gonzalez, *Phys. B*, 2001, **301**, 8–19.